Annual report Phase I: January 16, 2003-January 15, 2004

Iowa State University

NREL subcontract XDJ-2-30630-32

Executive summary

During this first year, we have concentrated on the following tasks.

1. Study of growth chemistry, device physics and defect densities in nanocrystalline Si solar cells for use as low bandgap cells in tandem cell structures.
2. Study of properties of a-Ge:H materials and devices for use as low bandgap cells in tandem cell structures.

Task 1.Nanocrystalline Si:H materials and cells

1.1 Study of growth chemistry of nanocrystalline Si solar cells

We set up a VHF diode plasma system, powered by a variable frequency function generator (Wavetek) and an RF amplifier (ENI), to study the growth and properties of nanocrystalline Si:H materials and devices. Most of the films were grown using 45 MHz discharge from mixtures of silane and hydrogen. The growth temperature was in the range of 250-450 C. The pressure in the reactor was varied between 50 mTorr and 500 mTorr. It is recognized that this is a lower pressure range than studied by most other workers using VHF. The objective of the study was to see how the plasma conditions affected the properties of the material. The structural and electronic properties such as activation energy were measured:

It was found from x-ray and Raman measurements that as the pressure increased, the crystallinity became worse for a given hydrogen dilution ratio [1]. Typical grain sizes ranged from 10 nm to 15 nm. The films were mostly <111> oriented. It was also found that the amount of hydrogen dilution necessary to produce highly crystalline films increased as the pressure increased. We also measured the plasma conditions using a Langmuir probe. It was found that at lower pressures, there was a higher flux of ions impinging on the substrate during growth, but the ion energy was still low, < 20 eV. From these results, we conclude, in contrast to other results [2], that low energy ion bombardment is beneficial for growing nanocrystalline films and devices with good properties. These results are described in greater detail in Appendix 1.

1.2 Measurement of defect densities, diffusion lengths and device I-V curves in nanocrystalline solar cells

Proof of concept solar cells were fabricated using the VHF and ECR discharges. The solar cells were of the p+nn+ type, with the n+ layer being deposited on a stainless steel substrate. The top p+ layer was contacted using an ITO layer. Light was incident on the cell through the ITO top layer. The ITO layer was deposited using sputtering in a 1% oxygen-99%Argon environment

in a sputtering system. The doped p+ and n+ layers were made using the ECR method described earlier, and the base n layer was made in either the VHF, or the ECR system. All the base layers studied were of n type doping, with significant doping concentrations, ~10^{15}/cm3 or larger. Therefore, it is not accurate to call these devices pin type, as is sometimes done. Rather, the correct terminology is to call them p+nn+ type.

The as-fabricated cells showed reasonably high fill factors, and voltages between 0.45 and 0.52 V, depending on the degree of crystallinity. The quantum efficiencies extended out to beyond 800 nm . No back reflector was used – just the polished stainless steel substrate.

The cells were measured for their dark I-V characteristics. The cells deposited using ECR process almost always showed a classical, two region I-V curves in the dark, an exp (qV/2kT) region and an exp(qV/kT) region, indicating the presence of a dominant defect level in the middle of the gap [3].

The defect densities in the cells were measured using low frequency capacitance techniques. As the frequency increased beyond about 400 Hz, the capacitance decreased, indicating that deepest levels were not responding. From this fact, we deduce that the deep levels were about 0.5 eV below the conduction band. The upper level of the dominant defect state was inferred from the frequency and voltage at which capacitance tended to saturate. From such measurements, we infer that upper boundary for the deep levels is about 0.35 eV below the conduction band.

The measurement of capacitance vs. voltage indicated that the slopes at low voltages were approximately twice the slope at high voltages. From these measurements, we deduce that the shallow levels (deduced from the slope at low voltages) are about equal in magnitude to the deep levels. This result is similar to what was observed at higher doping levels by Lips et al [4].We speculate that the same impurity, most likely oxygen, is causing both shallow and deep states. See Appendix 3.

The shallow donor densities could be changed by compensating with ppm levels of B during growth, using trimethyl B as the source for B. We discovered that as the shallow level density decreased, so did the deep level density, maintaining a rough one-to-one correlation between the densities of deep and shallow states, a remarkable observation. This observation supports the speculation earlier that the same impurity, most likely oxygen, was responsible for both deep and shallow states. It is known from the literature on c-Si that B tends to complex with oxygen during growth, and we speculate that a similar mechanism is occurring during the growth of nanocrystalline Si:H.

The details of device preparation, growth chemistry and defect measurements in ECR grown device samples are shown in Appendix 2. The graph showing the relationship between deep and shallow defects is shown in Appendix 3.

2. Material and Devices Properties in a-Ge:H

A-Ge:H is potentially a useful material for low gap solar cells, with almost a perfect bandgap for tandem-cell matching with a-Si:H as the high gap material. The problem to date has been the rather poor performance of these cells, with low fill factors. During this program, for the first time ever, we have succeeded in making good quality a-Ge:H materials and devices.

The materials and devices were fabricated using a low pressure ECR discharge technique. A significant amount of hydrogen dilution (30:1- 50:1) was used. Pressures in the reactor were

kept low (5 and 10 mTorr) in order to provide a significant ion bombardment to the growing surface.

The measurement of material properties, such as Urbach energy, subgap absorption and defect densities estimated from space charge limited current indicated that the valence band Urbach energy was in the range of 45-46 meV, and the midgap defect density was about 2-3x10^{16}/cm^3-eV. The latter value is still too high, by about a factor of 5-6, compared to the device quality a-Si:H films that we can make, but about an order of magnitude lower than reported in the literature.

p-i-n devices were made in these materials. The device measurements indicated that reasonable fill factors, of the order of 60%, could be achieved in these materials, along with voltages of ~0.42 V. The mobility-lifetime product of holes was measured using the reverse bias quantum efficiency technique, and was estimated to be in the range of 8x10^{-9} cm2/V, consistent with the increased defect density measured using SCLC technique.

The details of materials and device measurements are shown in Appendix 4 [5].

3. Measurements of defect density and diffusion length for nanocrystalline cells made by MV systems

We measured defect densities in nanocrystalline cells made by MV systems. We again find defect and doping densities to be approximately equal in these cells. The diffusion lengths of holes again correlated well with the defect density, with an increasing defect density leading to smaller diffusion lengths. See appendix 5. These results have been reported by MV systems separately to NREL, and also in a publication.[6].

Conclusion

In summary, during this first year of the program, we have achieved the following:

1. Growth of nanocrystalline Si:H materials using both ECR and VHF plasma techniques.
2. Understanding of plasma chemistry and the role of ions on the growth of nanocrystalline Si
3. Fabrication of nanocrystalline Si:H devices with good fill factors and voltages
4. Measurement of deep defects and doping in nanocrystalline Si:H
5. Control of defect density in nanocrystalline Si:H by compensation techniques
6. Measurement of diffusion lengths of holes in nanocrystalline materials and their correlation with defect density
7. Growth of high quality a-Ge;H
8. Measurement of defect density in a-Ge:H
9. Fabrication of good quality devices for the first time ever in a-Ge:H
10. Measurement of mobility-lifetime product of holes in a-Ge:H

In addition, a number of graduate students were educated and got their degrees in part based on NREL's support of this work. The students who graduated during this first year include:
Joshua Graves (M.S.)
Joshua Koch (M.S.)
Jianhua Zhu (Ph.D.)
These students add to the potential manpower base in photovoltaic technology in the U.S.

References

1. V. L. Dalal, J. Graves and J. Leib, Applied Physics Letters (to be published, 2004)

2. M. Kondo, Solar Energy Mater. And Solar cells, 78, 543(2003)

3. See, for example, B. Streetman and A. Banerjee, "Solid State Electronic Devices", 5th. Ed, Ch. 5 (Prentice Hall, NY 2001)

4. K. Lips, P. Kanshat, W. Fuhs, Solar Energy Mater. and Solar Cells, v 78, p 513-541(2003)

5. J. Zhu and V. L. Dalal, J. Non-Cryst. Solids (To be published, 2004)

6. Das, U.; Morrison, S.; Centurioni, E.; Madan, A. IEE Proc. Circuits and Devices, 150,282 (2003)

7. **Appendix 1**

Influence of pressure and ion bombardment on growth and properties of nanocrystalline Silicon materials

Vikram L. Dalal, Joshua Graves and Jeffrey Leib
Iowa State University, Dept. of Electrical and Computer Engineering
Ames, Iowa 50011
Email: vdalal@iastate.edu

Abstract

We report on the growth and properties of Nanocrystalline Silicon:H films deposited using plasma discharge at 45 MHz under varying pressure regimes from 50 mTorr to 500 mTorr. X-ray diffraction data revealed that the primary orientation in these films was <111>. The amount of hydrogen dilution needed to crystallize the films was found to be a strong function of deposition pressure, with significantly higher hydrogen dilution needed to crystallize films at higher pressures. Langmuir probe data showed that these results could be attributed to the increase in density of low energy hydrogen ions impinging on the substrate at lower pressures.

Nanocrystalline Silicon :H is an important material for solar energy conversion, thin film transistors and display devices [1-6]. It consists of small grains of Si, with H and a thin a-Si:H tissue passivating the grain boundaries [7,8]. Effective passivation of the grain boundaries reduces minority carrier recombination, and the achievement of diffusion lengths of the order of several micrometers [2,3]. The defect densities measured using ESR spectroscopy [9] or capacitance spectroscopy [10,11] are found to be in 10^{15} -10^{16}/cm^3 range. Most of the previous work on nanocrystalline Si:H has involved growth from a mixture of hydrogen and silane, using either RF (13.56 MHz) or VHF (40-100 MHz) plasma CVD process in a pressure range of 1-10 Torr, and a temperature range of 200-400 °C. It is generally found that one needs a very high dilution with hydrogen (>16-20:1) in order to grow crystalline as opposed to amorphous Si materials [2].

In this paper we examine the influence of pressure, power density and hydrogen dilution on the properties of nanocrystalline Si:H prepared using VHF discharge at 45 MHz and significantly lower pressures. We examine the structure using Raman and x-ray spectroscopy and also measure activation energies of films. It will be shown that pressure and power have a profound influence on the crystallinity achieved for a given degree of hydrogen dilution. Langmuir probes are used to characterize the plasma, and they show that low energy ion bombardment is important in achieving better crystallinity.

In Fig. 1, we plot the X-ray diffraction spectrum of a film. 2.4 micrometer thick, grown on stainless steel at a pressure of 50 mTorr with a hydrogen dilution ratio of 10:1. The dominant peak is <111>, not <220> in contrast to other work [2]. Grain size, deduced using Scherer's formula, is 15 nm. Grain size increased from 15 nm to 25 nm as the deposition temperature increased from 250 °C to 400 °C. The Raman spectrum for this film is shown in Fig. 2, with the prominent c-Si peak at ~520 cm^{-1}, and the amorphous phase at ~480 cm^{-1}. The ratio of the two peaks is 3.8:1, implying a high degree of crystallinity.

We also made films on Corning 7059 substrates for optical and conductivity measurements. The activation energy for conductivity and Raman spectra were measured for these films. An excellent correlation was obtained between the Raman peak ratio and the activation energy for conductivity; a low activation energy (~0.2 eV) corresponded to a high (>3.5:1) Raman peak ratio. In contrast, a high activation energy (~0.6-0.7 eV) corresponded to the presence of mainly amorphous shoulders in the Raman spectrum. The activation energy of our films did not vary with time, implying the absence of significant post-deposition oxidation.

Fig. 3 shows the relationship between the activation energy and hydrogen dilution for films grown at different pressures at 45 W power. Good crystallinity is observed in films grown at low pressures (50 and 100 mT) even at a low dilution ratio of 12:1. For films grown at 200 mTorr, one needs to increase hydrogen dilution to improve crystallinity. The films grown at 500 mTorr never became crystalline in the region of hydrogen dilution shown. By increasing the power level, we could make the higher pressure (200 mTorr)-grown films more crystalline, as shown in Fig. 4. A similar result was obtained for films grown at 500 mTorr, where it was found that it was necessary to have both high power (>70W) and high hydrogen dilution (>20:1) in order to crystallize the films.

The results of Langmuir probe measurements of the hydrogen plasma conditions near the substrate for depositions done at different pressures are shown in Fig. 5. As the pressure

decreases, the ion energy and ion density near the substrate increase. We believe that the presence of a higher density of low-energy ions at the substrate at lower pressures is the reason why the films are crystalline even at low hydrogen dilutions. The ion energies are not high enough to cause damage.

In conclusion, we have observed that, in contrast to previous results [12], low-energy ion bombardment improves the crystallinity of nanocrystalline Si:H films. The films produced at low pressures show a preferential <111> orientation. Good nanocrystalline films can be produced even at low hydrogen dilutions (10:1) at low pressures. We have also shown that low energy ion bombardment may lead to a higher degree of crystallinity.

This work was partially supported by a grant from NSF. We thank Max Noack, Kamal Muthukrishnan and Raegan Johnson for their help.

References

1. J. Meier, R. Fluckiger, H. Keppner and A. Shah, Appl. Phys. Lett., 65,860(1994)
2. A. V. Shah, J. Meier, E. Vallat-Sauvain, N. Wyrsch, U. Kroll, C. Droz and U. Graf, Solar Energy Mater. And Solar cells, 78, 469 (2003)
3. Kenji Yamamoto, Masashi Yoshimi, Yuko Tawada, Susumu Fukuda, Toru Sawada, Tomomi Meguro, Hiroki Takata, Takashi Suezaki, Yohei Koi, Katsuhiko Hayashi Solar Energy Mater. And Solar Cells, 74, 449-455 (2002)
4. M. Mulato, Y. Chen, S. Wagner and A. R. Zanatta, ,J.Non-Cryst. Solids,266-269,1260-1264(2000)
5. B. Rech, O. Kluth, T. Repmann, T. Roschek, J. Springer, J. Müller, F. Finger, H. Stiebig and H. Wagner, Solar Energy Mater. And Solar Cells, 74, 439-447(2002)
6. T. Brammer and H. Stiebig, J. Appl. Phys. , 94, 1035-1042 (2003)
7. W. Beyer, Solar Energy Mater. And Solar cells, 78, 235(2003)
8. U. Kroll, J. Meier, A. Shah, S. Mikahilov and J. Weber, J. Appl. Phys.,80,4971(1996)
9. K. Lips, P. Kanschat and W. Fuhs, Solar Energy Mater. And Solar cells, 78, 513 (2003)
10. V. L. Dalal, J. H. Zhu, M. J. Welsh and M. Noack, IEE Proc.-Circuits and Devices, 150, 316(2003)
11. V. L. Dalal, J. Graves, J. Koch and M. Ring, J. Non-Cryst. Solids (To be published, 2004)
12. M. Kondo, Solar Energy Mater. And Solar cells, 78, 543(2003)

Figure captions

1. x-ray diffraction spectrum of nanocrystalline Si film deposited on stainless steel substrate. The film has a dominant peak corresponding to <111> orientation. The peak at 45° is due to iron in the substrate.

2. Raman spectrum of the film whose x ray diffraction was shown in Fig. 1

3. The relationship of conductivity activation energy for nancorystalline Si:H films deposited on 7059 substrates as a function of hydrogen dilution for depositions done at different pressures. A low activation energy corresponds to a predominant crystalline phase whereas a high energy corresponds to a predominant amorphous phase. Note the interesting result for the film deposited at 200 mTorr which clearly shows improved crystallinity as hydrogen dilution increases.

4. The relationship between activation energy and power in the discharge for a fixed hydrogen dilution (15:1) for a film deposited at 200 mTorr. Note how increasing power tends to crystallize the film.

5. Langmuir probe data on ion flux and ion energy impinging on the substrate for VHF deposition done at 45 W as a function of deposition pressure. Note how both ion density and ion energy increase as the pressure reduces. At the pressures used, ion energy is still low enough to not cause ion bombardment induced damage.

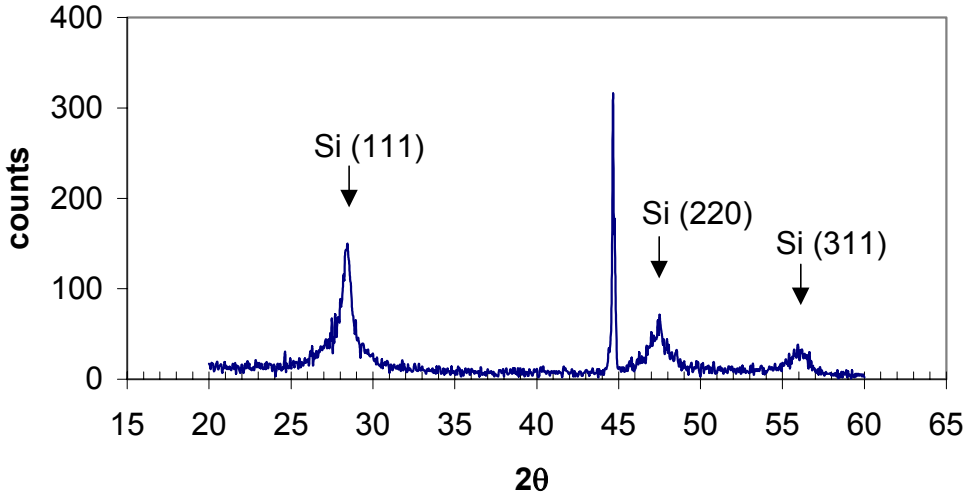
400
300
200
100
0
counts
Si (111)
Si (220)
Si (311)
15
20
25
30
35
40
45
50
55
60
65
2θ

Fig. 1

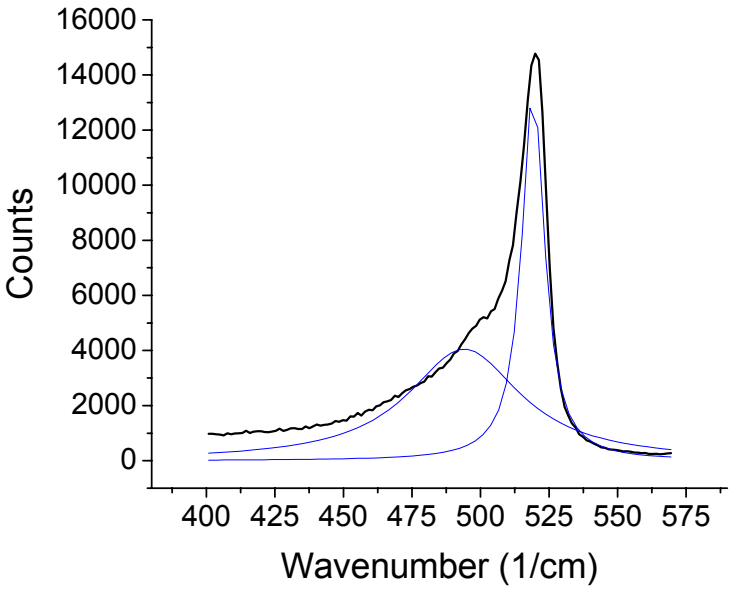
16000
14000
12000
10000
8000
6000
4000
2000
0
Counts
400
425
450
475
500
525
550
575
Wavenumber (1/cm)

Fig 2

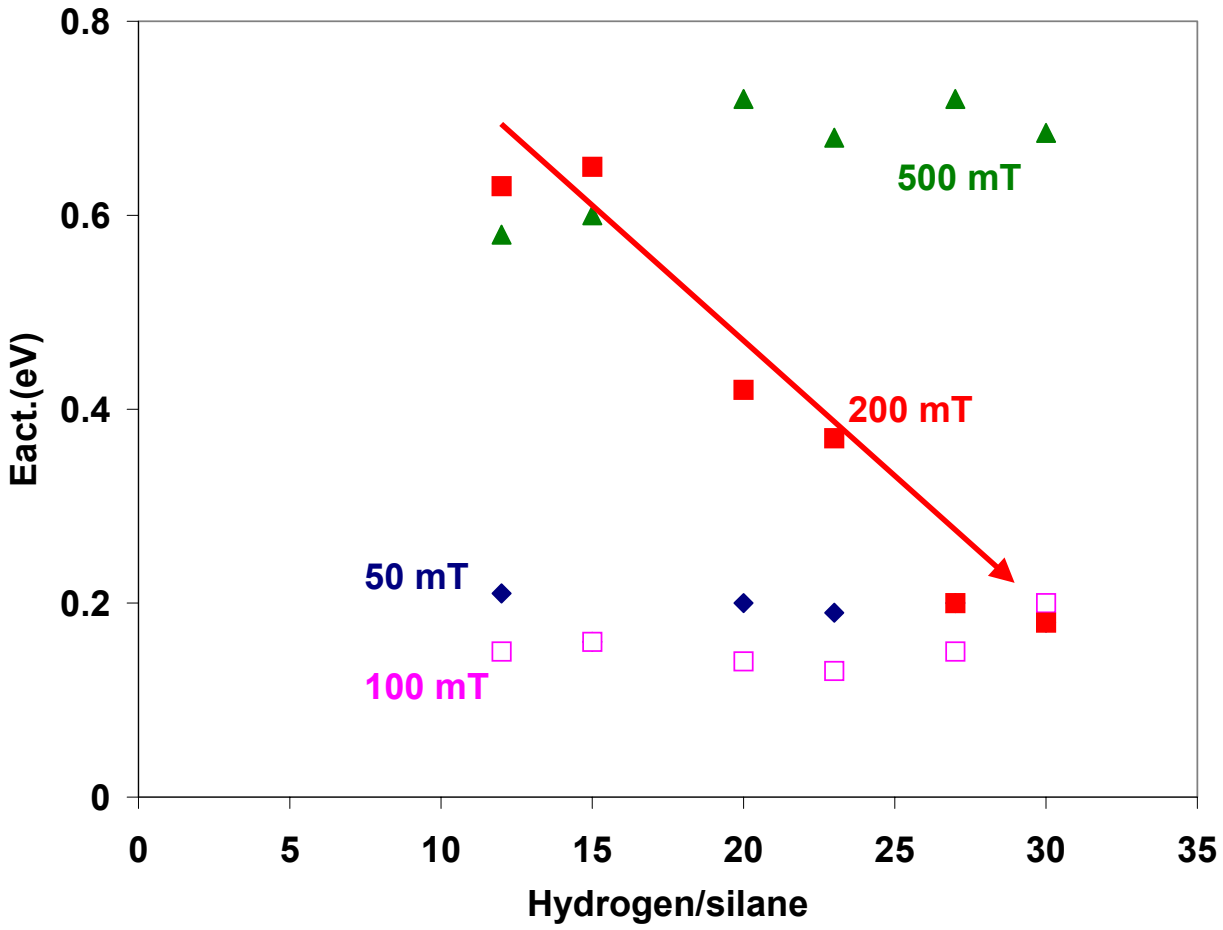
0.8
0.6
0.4
0.2
0
Eact.(eV)
0
5
10
15
20
25
30
35
Hydrogen/silane
500 mT
200 mT
50 mT
100 mT

Fig. 3

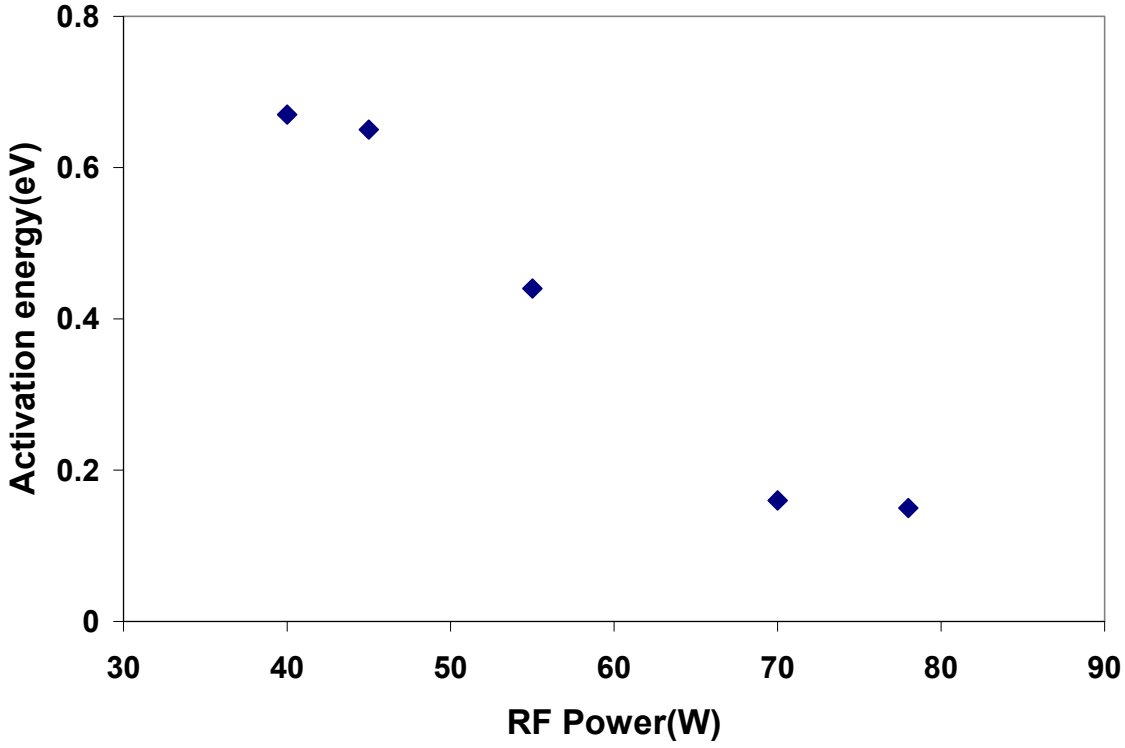

Fig. 4

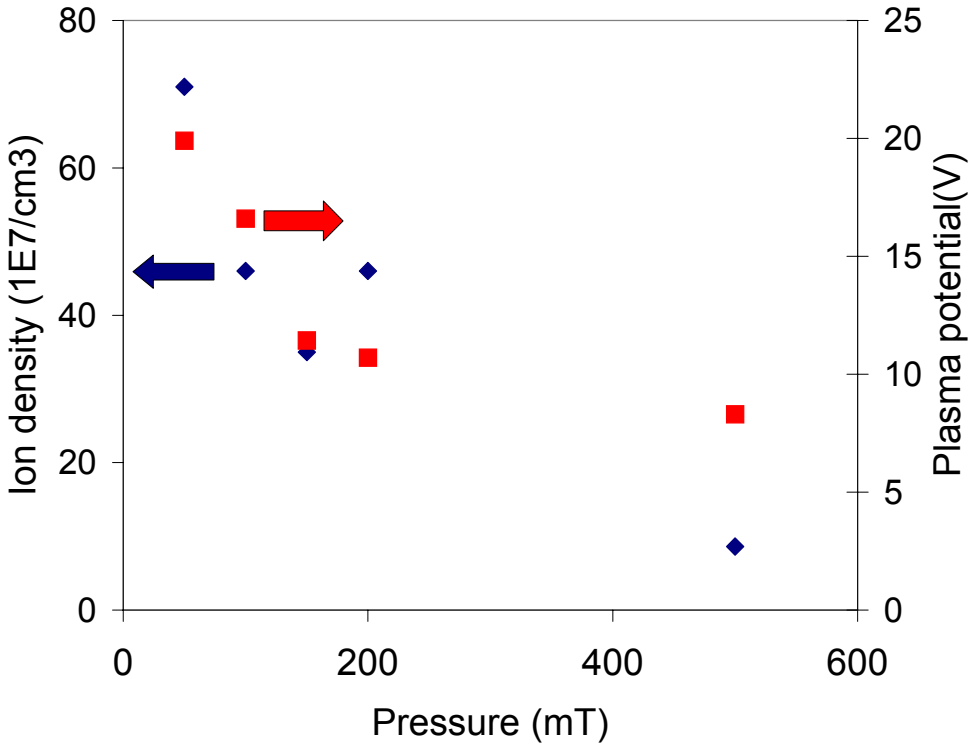
80
60
40
20
0
Ion density (1E7/cm3)
25
20
15
10
5
0
Plasma potential(V)
0
200
400
600
Pressure (mT)

Fig. 5

Appendix 2.

Microcrystalline Silicon:H Solar Cells Fabricated Using ECR Plasma Deposition

Vikram L. Dalal, J. H. Zhu, Matt Welsh and Max Noack
Iowa State University
Microelectronics Research Center
Ames, Iowa 50011, USA
email: vdalal@iastate.edu

Abstract

We report on the properties of microcrystalline Si:H materials and solar cells fabricated using remote, low pressure ECR (Electron-Cyclotron-Resonance) plasma deposition. p+nn+ junction solar cells were deposited at ~ 275-325 C on stainless steel substrates using mixtures of silane and hydrogen. Microcrystalline layers and solar cells could be produced even for low dilution ratio of hydrogen/silane of 8:1. It was found that once the crystallization started, one could decrease the hydrogen/silane ratio and still obtain microcrystalline Si:H solar cells. The voltage of the solar cells could be improved by tailoring the interface between p+ and n layers. An amorphous interfacial layer improved the voltage. A thin amorphous Si:H layer at the back, between n+ and n layers was used to significantly reduce the shunt resistance. Standard device analyses, including dark I(V) curves and capacitance measured at several frequencies revealed that the device characteristics could be understood in terms of a standard Si diode model. The doping densities in the n layer were found to be in the $1x10^{15}$ to $2x10^{16}$/cm3 range and could be adjusted by adjusting the amount of compensatory B doping of the layer. The influence of addition of He dilution to the mixture was also studied, and it was found that He degrades the crystallinity, though it increases the growth rate and open-circuit voltage.

I. Introduction

Microcrystalline Si:H is an important technological material which is being used extensively for solar cells and thin-film transistors [1-4]. Basically, it is a small grained Si material, the grain size being approximately 10 nm, with grain boundaries saturated with H or with thin a-Si:H tissue layers separating grains [5-7] . The presence of significant H bonding at the grain boundaries, and the presence of the thin amorphous tissue, leads to excellent minority carrier transport through the grains and minimizes grain boundary recombination. The optical absorption characteristics of the material are similar to that of crystalline Si, with an enhancement due to internal scattering at the grain boundaries [8]. In contrast to a-Si:H, most microcrystalline Si:H materials and devices are very stable against light-induced degradation, although some material with excessive porosity do suffer from rapid oxidation and changes in device characteristics.

Four techniques have been used in the past to deposit microcrystalline Si:H solar cells, namely standard glow discharge at 13.56 MHz [9], VHF discharge at higher frequencies,[10,11], hot wire deposition[12,13], and low pressure, remote electron-cyclotron-resonance (ECR)

plasma deposition. Our group has used the latter technique to deposit films and devices in both microcrystalline Si:H and microcrystalline (Si,Ge):H [14-18]. In this paper, we explore device fabrication techniques for ECR-deposited microcrystalline Si:H solar cells, and show that appropriate design of both the back (n^+n) and front (p^+n) interfaces can significantly improve the device properties. We also study the dark I(V) characteristics of these devices, and capacitance-voltage spectroscopy at different frequencies, and show that the ECR-deposited base n layers in solar cells behave very similarly to standard crystalline Si materials. The ECR-deposited cells are found to be very stable against both environment-induced oxidation and light soaking, with reproducible results being obtained three years after initial deposition.

II. Growth of materials and solar cells

The materials and solar cells were prepared using the remote, low pressure ECR plasma technique previously described [14]. Fig. 1 shows a schematic diagram of the reactor system used. A beam of hydrogen ions and radicals is produced using an ECR plasma and travels towards the substrate, which is about 25 cm away from the resonance zone. Silane is introduced near the substrate. Some silane diffuses upstream towards the plasma resonance zone; however, the reactions products of silane produced upstream do not contribute to growth since their mean free paths are much smaller than the resonance zone-substrate distance of 25 cm. The electrons and ions in the plasma interact with silane near the substrate and give rise to film producing radicals. The ECR plasma deposition technique has some unique advantages compared to the standard RF glow discharge technique. Among these advantages are:

1. The plasma can be maintained at very low pressures because of the very long mean free path of the electrons rotating around the magnetic field lines. The advantage of low pressures is that there is little reaction in the gas phase between the different radicals (e.g. SiH_2 and SiH_3) generated by the plasma. This means that higher order radicals, such as Si_2H_5, do not play a role in growth, which makes the film more homogeneous. Indeed, we have previously shown that only the three silane radicals, SiH, SiH_2 and SiH_3, play a role in growth of films in the ECR reactor [19].
2. The ECR plasma, because of the high frequency involved (2.45 GHz), produces ions of only about 10-15 eV energy [21] , considerably less than the energy of ions in a RF glow discharge reactor which can approach 50-100 V under conditions typically used for microcrystalline Si:H growth.
3. The fact that the resonance zone is remote from the substrate allows for a good control over the energy and density of the arriving species at the substrate, which may play a role in promoting crystallization. For example, by controlling pressure, one can change the ratio of H*/H2 arriving at the substrate [21], with higher pressure leading to a smaller ratio. We find, indeed, that when H*/H2 ratio at the substrate decreases, one obtains an amorphous film as opposed to a microcrystalline film.

The incident microwave power in the reactor was maintained at ~ 200 W. The substrate temperature was varied between 270 C and 370 C. No significant differences in the properties of the films and devices were observed so long as the temperature was below about 340 C. However, increases in temperature beyond ~ 350 °C led to reductions in open-circuit voltage. This may be related to a loss of hydrogen from either the Si-H bonds at the grain boundaries or from the a-Si:H tissue coating the grain boundaries at higher temperatures.

One of the experimental factors investigated was the ratio of hydrogen/silane. In contrast to other groups, we find that excellent films and devices can be grown even when the hydrogen/silane ratio is as low as 8:1, although more typically, we used a ratio of about 10:1. We believe that the beneficial effects of low energy ion bombardment may be responsible for our being able to use a lower dilution ratio of hydrogen to silane. This lower dilution allows us to grow the materials and devices at higher growth rates (~3Å/sec). Even higher growth rates (up to 10 Å/s) can be obtained if He is used in addition to hydrogen. We will briefly discuss the properties of solar cells made using He and hydrogen dilutions. Small amounts of Boron (sub-ppm levels) are added to the mixture so as to compensate for the inevitable oxygen donors present in plasma reactors.

III. Device Structure

The basic device structure is shown in Fig. 2. It consists of a polished, non-textured, steel substrate. A 100 nm thick n^+ a-Si:H layer is first deposited to form the back contact. Next, a thin (20-50 nm) undoped a-Si:H layer is deposited. We discovered that the presence of this thin a-Si:H layer helped seal up any shorts and significantly improved the device properties such as shunt resistance. Next, the n microcrystalline Si:H base layer is deposited to the given thickness, typically about 0.8-1.0 micrometer thick. This is followed by a thin, graded gap interfacial buffer layer to provide for bandgap matching between the n layer and the p^+ layer and also to reduce any electron recombination at this interface. The previous buffer layer we had used was an amorphous layer, whose bandgap was varied between ~1.4 eV to 1.8 eV by changing the Ge:Si:C ratios[17]. In this work, we report a buffer layer which is in two parts. First, the amorphous/crystalline fraction in the interfacial layer is increased continuously by increasing the silane flow (from 1:10 silane:hdyrogen ratio to 1:6 ratio) as we proceed towards the p layer. This crystalline layer with decreasing crystallinity is approximately about 100 nm thick. It is followed by an amorphous (Si,C) layer whose function is to match the base layer to the p-a-(Si,C):H layer. The amorphous (Si,C) buffer layer is very thin, about 15-30 nm. If it is too thick, or if too high a bandgap is used for a-(Si,C):H, inflection points occur in the I(V) curve. This point will be discussed later. The final active layer is a p^+ a-(Si,C):H layer deposited at lower temperatures (170 °C). A sputtered ITO contact completes the cell. The thickness of the base n layer was generally in the range of 0.8 – 1 .0 micrometer when only hydrogen was used, but was higher (~2.0 micrometer) when He was also used as a diluent gas.

The energy band diagram of the cell is shown in Fig. 3. It is seen that, unlike the case for a-Si:H cells, this band diagram resembles a standard crystalline Si p^+nn^+ junction solar cell. Unlike a-Si:H, the electric field does not extend over the entire thickness of the n layer. Nor is the base layer undoped; it is rather n-doped. In our cells, and in cells made by MV Systems (a company in Golden, Colorado) that we measured [20], capacitance data revealed that the so called i layers were really n layers. Therefore, there is no point in calling the cells p-i-n, as some authors do. The doping in these base layers is quite high, in the 10^{15} to 2.5×10^{16} / cm^3 range. Note that the presence of amorphous n^+ and p^+ layers alters the band diagram from that used for standard c-Si devices. It will be recognized that the presence of a n^+ a-Si:H back layer is potentially very useful in allowing for efficient transfer of photons after reflection back into the crystalline base layers, though we do not use any efficient light trapping or back reflection

techniques for our cells as yet. The back amorphous layers also serve to reduce shorts and increase shunt resistance, while having minimal effects on series resistance.

IV Device Results and Influence of p+n interface layer

The I(V) curve for one of our better devices is shown in Fig. 4. The devices are quite reproducible, (voltages and fill factors within 5%), except for the few which suffer from the inevitable pinholes. The efficiency, without any significant back reflection and no deliberate light trapping, is ~4.7%, with voltage of 0.48V and fill factor of 0.7. The corresponding quantum efficiency (QE) curve is shown in Fig.5, showing the QE from 400 to 800 nm. A more detailed QE curve, showing that the QE follows the absorption of c-Si out to 1.1 eV energy is shown in Fig. 6. For comparison, we also show the absorption coefficient for a crystalline Si wafer over the same range of energy. Thus, it is confirmed that the base layer in the device is primarily microcrystalline Si:H.

The devices are extremely stable against both exposure to room air, and against light-induced degradation. Some of the devices have now lasted about 3 years in ambient atmosphere with essentially the same I(V) curves being reproduced over time, showing that there is no ambient-induced oxidation and degradation in these devices. We believe that this result may be a consequence of the fact that the films and devices are subjected to ~10-15 eV ion bombardment during growth [21], thereby producing dense materials resistant to oxygen percolation along grain boundaries.

The influence of changing the hydrogen/silane ratios was studied. In Fig. 7, we show that as the silane/hydrogen ratio increases, the open-circuit voltage increases. We can still get good microcrystalline cell characteristics even at silane/hydrogen ratios of 1:8, in contrast to the results of other groups where for higher silane content beyond about 1:16 ratio, the material became primarily amorphous[11]. As the voltage increases, the QE at 800 nm decreases, indicating more amorphous-like nature to the basic n material; see Fig. 7.

We also studied the influence of varying the thickness of the interfacial buffer layer for a fixed composition microcrystalline n base layer. In Fig. 8, we show the influence of increasing the thickness of the a-(Si,C):H buffer layer from 15 nm to 30 nm on the I(V) curve. Clearly, the voltage has increased as the buffer layer thickness increases, but the fill factor decreases drastically. In extreme cases, the decrease in fill factor shows up most prominently as an inflection point in I(V) curves, indicating troubles with hole collection as the electric field across the interfacial layer decreases. This results may be a consequence of the fact that as one adds C to the buffer layer, or makes the buffer layer more amorphous, the valence band edge moves down with respect to the microcrystalline Si:H layer, forming a notch to trap the holes (See Fig. 9 for an energy band diagram showing the notch). Previously, we had shown that such a notch results even for a-Si:H cells when an improper graded gap a-(Si,C):H buffer layer is used.[22]. If the thickness of the buffer layer is too high, the holes cannot tunnel through this notch, particularly in forward bias (power quadrant). This effect does not show up in reverse bias because the fields are high, assisting in tunneling across the notch. It also does not show up in far forward bias, because the holes are now being injected from the p into the n layer, and they do not get trapped by the notch. We recognize that this is only a qualitative model; an exact quantitative model will require a measurement of band edge discontinuities between microcrystalline Si and a-(Si,C):H using internal photo-emission type experiments.

Finally, we studied the addition of He to the mixture to increase the growth rates to ~5 A/s rate. In Fig. 10, we show the I(V) curve for such a device. The thickness of the n layer in this cell is ~1.0 micrometer; the fill factor is still reasonable (0.67) indicating reasonable diffusion length. However, QE data reveal that the QE at 800 nm has actually decreased to 0.04 compared to a device with similar thickness made with hydrogen dilution alone where the QE at 800 nm was 0.07. This decrease is a clear indication that the material has become more amorphous like and less crystalline, a result which agrees with Raman measurements on films which show more amorphous structure as He is added to the gas mixture. The voltage generally increases as more He is added, another indication that the material is becoming more amorphous like.

V. Device Analysis and Material Measurements

It is well known that in a-Si:H devices, measurement techniques, such as C(V) curves, can lead to misleading results unless one is careful about using the right temperature-frequency regime. This fact arises from the nature of the a-Si:H material, where there is a continuous distribution of deep states, extending across the bandgap range. During a C(V) measurement, the states which are ~0.8-0.9 eV below the conduction band do not respond to standard measurement frequencies. For a state ~0.85 eV below the conduction band, one can calculate the attempt-to-escape frequency ν from :

$$\nu = \nu_o \exp [-(E_c - E_t)/kT] \quad \ldots\ldots\ldots\ldots\ldots\ldots\ldots\ldots\ldots\ldots\ldots\ldots \quad (1)$$

ν for the 0.85 eV deep state is 5.6×10^{-4} /sec, using the standard value of 1×10^{11}/sec for ν_o.(If we were to use a value of 1×10^{12}/s for ν_o , as some authors have used [23], the escape time would be 5.6×10^{-3} sec, still requiring sub 1 Hz frequency in C(V) measurements). Therefore, to see such a state, one would have to use frequencies of 0.0002 Hz, or use higher temperatures. For microcrystalline Si:H, since the bandgap is 1.1 eV, the mid-gap deep state levels are only about 0.5 eV from the conduction band, and $\nu \sim 413$ Hz. Therefore, a measurement at 100 Hz should yield meaningful data about the total defect and donor density. Of course, if there were few deep states, then a measurement at higher frequencies would not be too different from a measurement at 100 Hz. In this case, a measurement at 50 C or 75 C should also yield results similar to the ones obtained at 25 C.

We have measured the C(V) curves of our devices at 100 Hz,120 Hz, 1 kHz and 10 kHz using a Stanford Research System C(V) meter. The signal voltage was kept small, 0.1V. The capacitance as a function of frequency is shown in Fig. 11, showing that there is little change in capacitance at low frequencies upto 1 kHz, but it reduces by about 2x at 10 kHz, as expected. In all cases, care was taken to make sure that true parallel-circuit capacitance was being measured; i.e. the shunt resistance was high enough (~100 kohms). If the shunt resistance is low (< 1 kohm), accuracy of the measurement significantly decreases.

In Fig. 12, we plot the results of a C(V) curve on one of our normal, high fill factor (>0.65) devices. The total defect density is ~ $2 \times 10^{16}/cm^3$,and the shallow donor density is about half of that, or 1×10^{16}/cm3. The built-in voltage is approximated to be ~0.8 V, as expected for this doping density in Si.

We also measured the dark I(V) curves in our device. The I(V) curve is shown in Fig. 13, and it can be fitted extremely well to a standard Si diode three-regime curve, one representing current arising from generation-recombination in the depletion region ($I \sim qV/2kT$) , one representing diffusion-dominated current ($I \sim qV/kT$), and one representing the series resistance of the base layer. This point is made clearer by replotting the exponential data as the sum of two exponential curves, one representing exp(qV/2kT) and one, exp (qV/kT). See Fig. 14. Thus, unlike the results of some other groups [10], we do not get strange I(V) curves with varying diode factors. Rather, we get the standard result expected for c-Si, in agreement with the standard capacitance results.

The combination of standard dark I(V) curve and standard C(V) curve, virtually independent of temperature and frequency in the range studied, clearly indicates that the band diagram shown in Fig. 3 is the correct band diagram, representing a crystalline type device. In the accompanying paper from MV Systems, they show that their capacitance and diode dark current data can also be fitted with this standard model[20].

Note that in the companion paper from MV Systems [20], we also measured diffusion lengths using a reverse-biased QE technique for a double-transparent cell. The diffusion length was found to be 1.2 micrometer in their material whose doping density is in the $10^{15}/cm^3$ range. Since our cells are deposited on non-transparent substrates, such measurements are difficult to make; we are now in the process of making double transparent structures for our cells.

VI. Conclusions

In conclusion, we have shown that ECR deposition at low pressures can lead to the growth of high quality microcrystalline Si:H solar cells. The solar cells are very stable against both light induced and environment-induced degradation. The base layers in the cell behave very similarly to the base layers in crystalline Si solar cells, with dark currents being controlled by the standard diode generation-recombination and diffusion models. The measurement of capacitance vs. voltage curves at low frequencies (100 Hz) yields doping densities in the 1×10^{15}- $2.5 \times 10^{16}/cm^3$ range. The capacitance does not change significantly as the frequency is increased to 1kHz, and then changes only by a factor of 2, indicating that the deep lying defect density is comparable to the donor density. The performance of the solar cells can be improved by appropriate design of the p-n interfacial layer, with a graded amorphous interfacial layer leading to higher voltages. Too thick an interfacial layer possibly leads to a notch in the valence band which may result in poor hole transport and a poor fill factor, with perhaps even an inflection point in the I(V) curve. A thin back amorphous Si layer next to a-Si n+ layer improves the shunt characteristics of the cell. We find that good devices can be made even when the hydrogen/silane dilution ratio is only about 8:1, though more typically, we use a ratio of 10:1. We can make good cells using a mixture of He and hydrogen dilution. As He/hydrogen ratio increases, the QE at 800 nm decreases and the open circuit voltage increases.

VI. Acknowledgements

This work was partially supported by a sub-contract from National Renewable Energy Laboratory. We thank Josh Koch, Puneet Sharma, Keqin Han and Durga Panda for their technical help.

References

1. Kenji Yamamoto, Masashi Yoshimi, Yuko Tawada, Susumu Fukuda, Toru Sawada, Tomomi Meguro, Hiroki Takata, Takashi Suezaki, Yohei Koi, Katsuhiko Hayashi " Large area thin film Si module", Solar Energy Mater. And Solar Cells, 74, 449-455 (2002)

2. B. Rech, O. Kluth, T. Repmann, T. Roschek, J. Springer, J. Müller, F. Finger, H. Stiebig and H. Wagner "New Materials and deposition techniques for highly efficient silicon thin film solar cells", Solar Energy Mater. And Solar Cells, 74, 439-447(2002)

3. M. Mulato, Y. Chen, S. Wagner and A. R. Zanatta, "Microcrystalline Si with high electron field-effect mobilityd eposited at 230 C", J.Non-Cryst. Solids,266-269,1260-1264(2000)

4. Y. Chen, K. Pangal, J. C. Sturm and S. Wagner, J.Non-Cryst. Solids, 266-269,1274-1278(2000)

5. O. Vetterl, A. Groß, T. Jana, S. Ray, A. Lambertz, R. Carius and F. Finger, "Changes in electric and optical properties of intrinsic microcrystalline silicon upon variation of the structural composition", J. Non-Cryst. Solids, 299-302,p.772-777 (2002)

6. T. Unold, R. Brüggemann, J. P. Kleider and C. Longeaud "Anisotropy in the transport of microcrystalline silicon", J. Non-Cryst. Solids, 266-269,325-330(2000)

7. J. Kocka, H. Stuchlíková, J. Stuchlík, B. Rezek, T. Mates, V. Vrk, P. Fojtík, I. Pelant and A. Fejfar, "Model of transport in microcrystalline silicon", J.Non-Cryst. Solids, 299-302,355-360(2002)

8. Vanacek M., Poruba A., Remes Z., Rosa J., Kamba S., Vorlicek V., Meier J. and Shah A., " Electron spin resonance and optical characterization of defects in microcrystalline Si", J.Non-Cryst. Solids, 266-269, p. 519-523(2000)

9. Y. Nasuno, M. Kondo and A. Matsuda, "Microcrystalline silicon thin-film solar cells prepared at low temperature using PECVD", Solar Energy Mater. And Solar Cells, 74, 497-503(2002)

10. O. Vetterl, F. Finger, R. Carius, P. Hapke, L. Houben, O. Kluth, A. Lambertz, A. Mück, B. Rech and H. Wagner, " Intrinsic microcrystalline silicon: A new material for photovoltaics", Solar Energy Mater. And Solar Cells, 62, 97-108(2000)

11. J. Meier, S. Dubail, S. Golay, U. Kroll, S. Faÿ, E. Vallat-Sauvain, L. Feitknecht, J. Dubail and A. Shah, "Microcrystalline silicon and the impact on micromorph tandem solar cells", Solar Energy Mater. And Solar Cells, 74, 457-467(2002)

12. S. Klein, F. Finger, R. Carius, B. rech, L. Houben, M. Luysberg and M. Stutzmann, " High efficiency thin film solar cells with intrinsic microcrystalline Si prepared by hot wire CVD", Mat. Res. Soc. Symp. Proc. Vol. 715, A26.2(2002)

13. P. A. T. T. van Veenendaal, C. M. H. van der Werf, J. K. Rath and R. E. I. Schropp "Influence of grain environment on open circuit voltage of hot-wire chemical vapour deposited Si:H solar cells", J. Non-Cryst. Solids, 299-302, p. 1184-1188(2002)

14. V. L. Dalal, S. Kaushal, E. X. Ping, J. Xu, R. Knox and K. Han, "Microcrystalline and mixed-phase Si:H: Preparation, properties and potential for devices", Proc. of Mater. Res. Soc. 377, 137(1995)

15. K. Erickson and V. L. Dalal, "Growth of microcrystalline Si:H and (Si,Ge):H films on polyimide substrates using ECR deposition techniques", Proc. of Mater. res. Soc., 467, 409(1997)

16. K. Erickson and V. L. Dalal, "Preparation and properties of microcrystalline (Si,Ge) on plastic substrates" , Proc. of MRS, 507, 987(1998)

17. V. L. Dalal and K. Erickson " Microcrystalline Si solar cells", Proc. Of MRS, Vol. 609(2000)

18. V. L. Dalal and K. Erickson, " Microcrystalline Si and (Si,Ge) solar cells on plastic substrates", Proc. Of 28th. IEEE Photovolt. Spec. Conf.(2000) ,p.792-795

19. M. Pontoh, Vikram Dalal and Neha Gandhi, "Characterization of ECR plasma", Proc. Of Mater. Res. Soc. (2002) Vol. 715

20. U. Das et al, this issue

21. S. Kaushal, V. L. Dalal and J. Xu, "Growth of high quality a-(Si,Ge):H films using low pressure remote ECR discharge, J. Non-Cryst. Solids, 198-200, 563(1996)

22. V. L. Dalal and G. Baldwin, " Design and fabrication of graded bandgap solar cells in a-Si and alloys", Proc. of Mater. Res. Soc., 297, 833(1993)

23. R. A. Street, "Hydrogenated amorphous Si", (Cambridge University Press, 1993)

Figure Captions

1. Schematic diagram of the ECR plasma reactor used to grow microcrystalline Si:H. devices. It is a single chamber machine, operated in a remote plasma mode at pressures of ~5 mTorr. Hydrogen is introduced upstream near the microwave inlet, and silane downstream near the substrate.

2. A schematic diagram of the basic device, deposited on untextured steel substrates.

3. Band diagram of the device, showing the back thin n+-n interfacial a-Si:H layer, the n microcrystalline Si:H base layer and the graded gap buffer layer at the p+-n interface. The field does not extend across the entire base layer.

4. I(V) curve for a microcrystalline Si:H cell with a base layer thickness of ~0.8 micrometer

5. Quantum efficiency of cell of Fig. 4 plotted vs. wavelength

6. Quantum efficiency of a cell plotted on log scale, and absorption coefficient of Si, both plotted vs. energy, showing crystalline Si type absorption behavior in the microcrystalline cell at low energies. The deviation in QE at high energies may be a result of absorption in the back amorphous layer and enhanced scattering at grain boundaries.

7. Open circuit voltage and QE at 800 nm vs. silane /hydrogen ratio used to grow the base layer

8. Influence of increasing the thickness of p-n buffer layer to 30 nm on I(V) curve. The case for a 15 nm buffer layer was shown in Fig. 4. In extreme cases, an inflection point may occur in the I(V) curve.

9. Proposed band diagram at p-n interface showing the development of a notch as the bandgap of buffer layer is increased. The notch traps holes, and a thick notch prevents tunneling of photo-generated holes into the p layer when electric field is reduced in the power quadrant.

10. I(V) curve of a cell made with a base layer fabricated with Helium dilution in addition to hydrogen dilution .

11. Capacitance-voltage curve for a standard device vs. frequency

12. Capacitance voltage curve of a device, showing classical crystalline Si type behavior, with a doping density of $2.2 \times 10^{16}/cm^3$,and a built-in voltage of 0.8 V

13. Dark I(V) curve for a device, showing three regions, a generation-recombination at low voltages, a diffusion at higher voltages, and a resistive loss at the highest voltages. The curves indicate a classical c-Si type behavior.

14. Detailed analysis of I(V) curve of Fig.13, showing the two diode regions. The exp(qV/kT) curve is generated by taking the actual I(V) data and subtracting the exp (qV/2kT) data from it.

Fig. 1

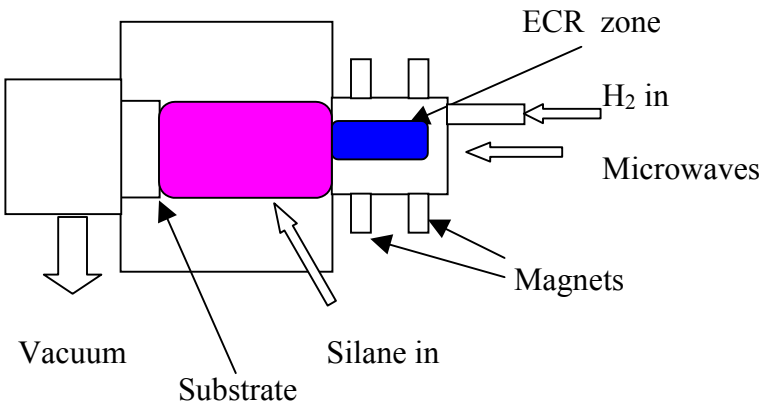
ECR zone
H_2 in
Microwaves
Magnets
Vacuum
Substrate
Silane in

Fig. 2

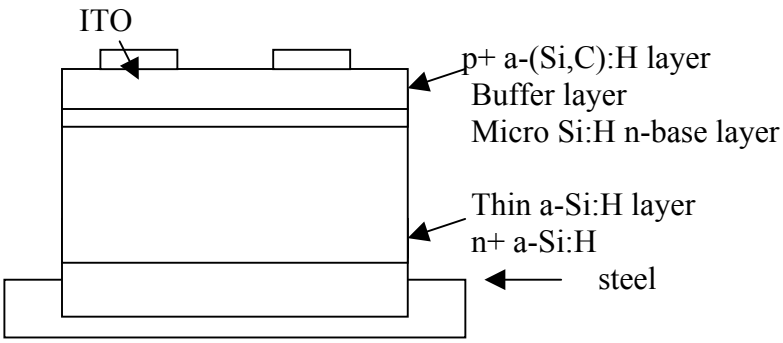
ITO
p+ a-(Si,C):H layer
Buffer layer
Micro Si:H n-base layer
Thin a-Si:H layer
n+ a-Si:H
steel

Fig. 3

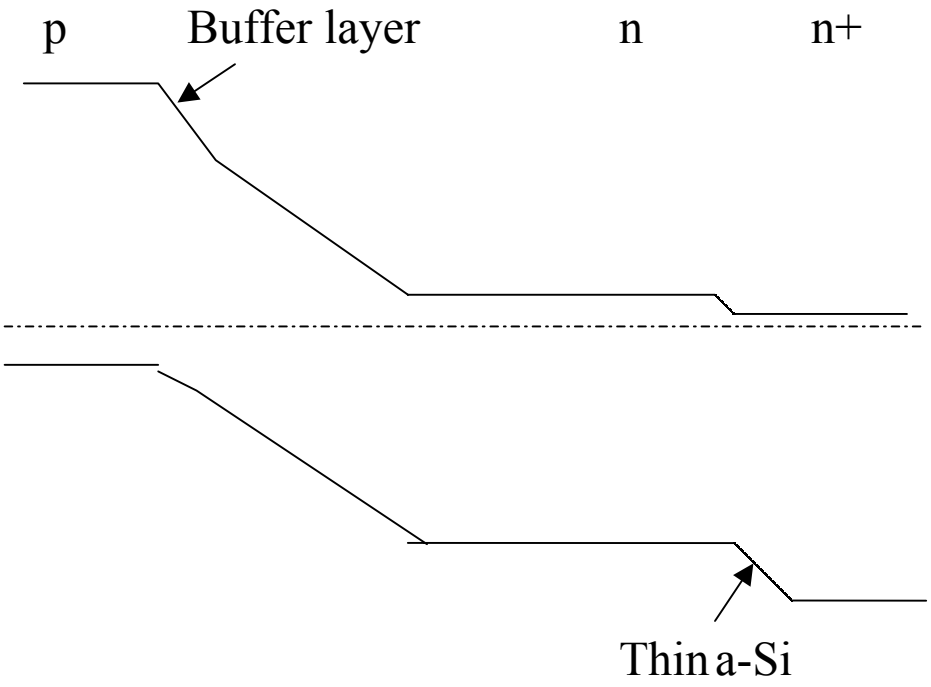

Fig. 4

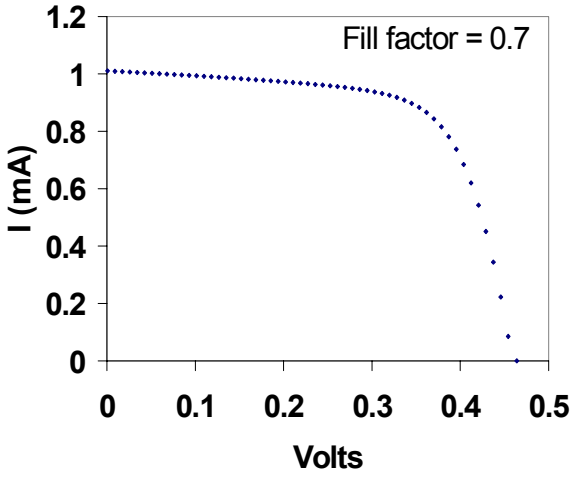

Fig. 5

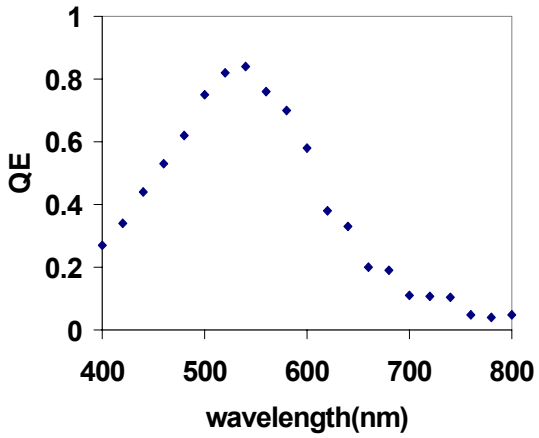

Fig. 6

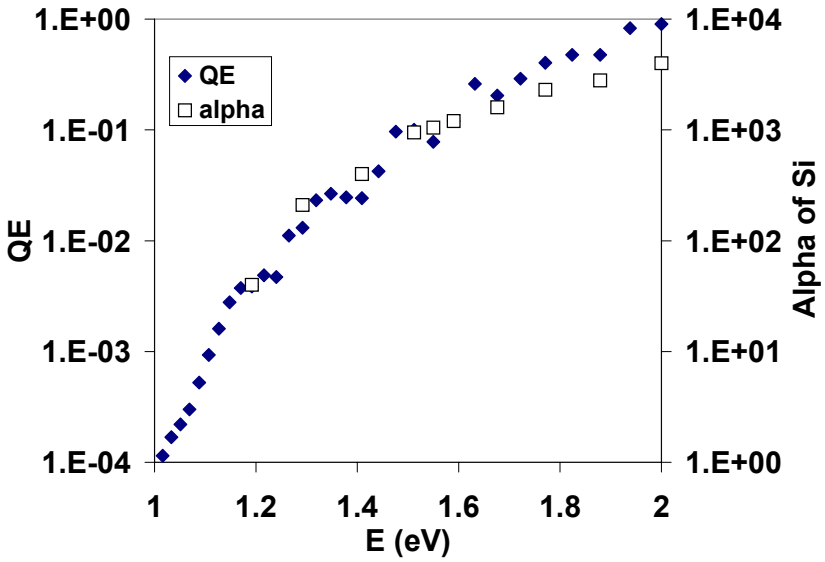
1.E+00
1.E-01
1.E-02
1.E-03
1.E-04
QE
1.E+04
1.E+03
1.E+02
1.E+01
1.E+00
Alpha of Si
QE
alpha
1
1.2
1.4
1.6
1.8
2
E (eV)

Fig. 7

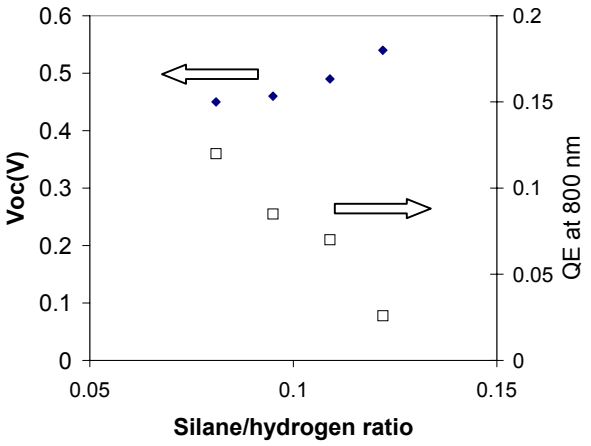
0.6
0.5
0.4
0.3
0.2
0.1
0
Voc(V)
0.2
0.15
0.1
0.05
0
QE at 800 nm
0.05
0.1
0.15
Silane/hydrogen ratio

Fig. 8

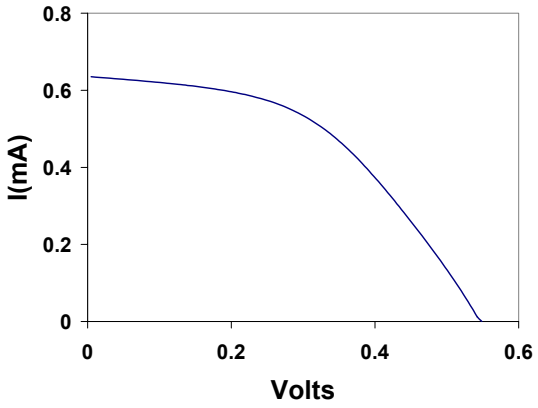

Fig. 9

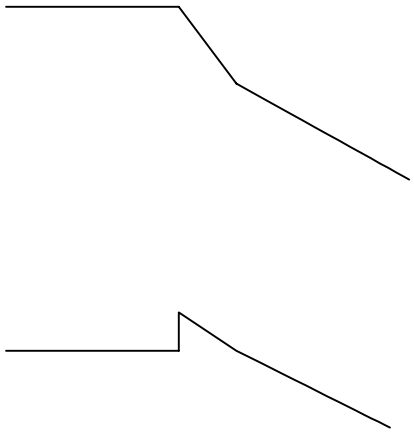

Fig. 10

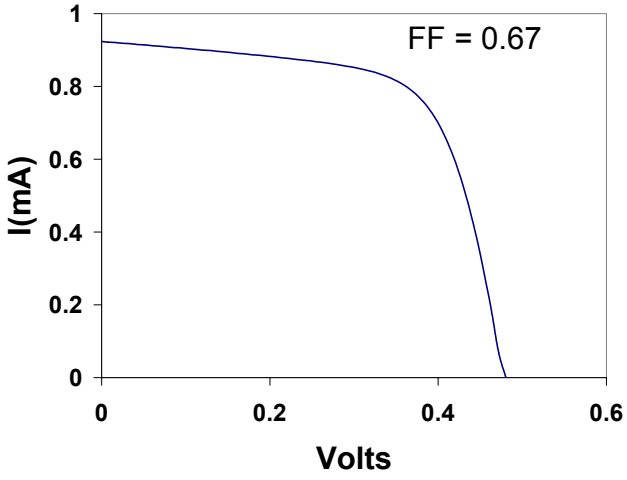

Fig. 11

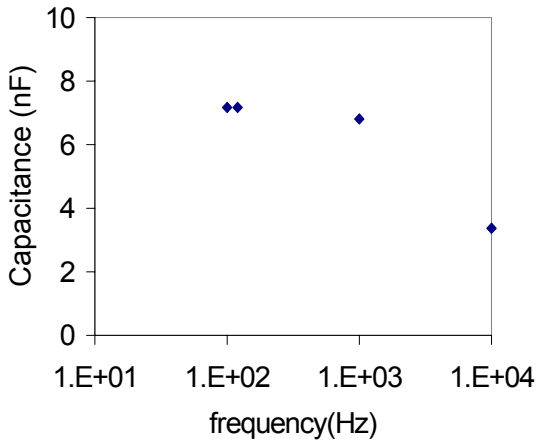

Fig.12

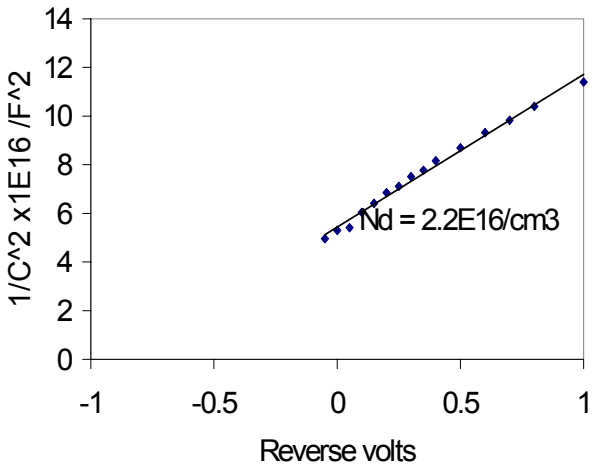
14
12
10
8
6
4
2
0
1/C^2 x1E16 /F^2
-1
-0.5
0
0.5
1
Reverse volts
Nd = 2.2E16/cm3

Fig. 13

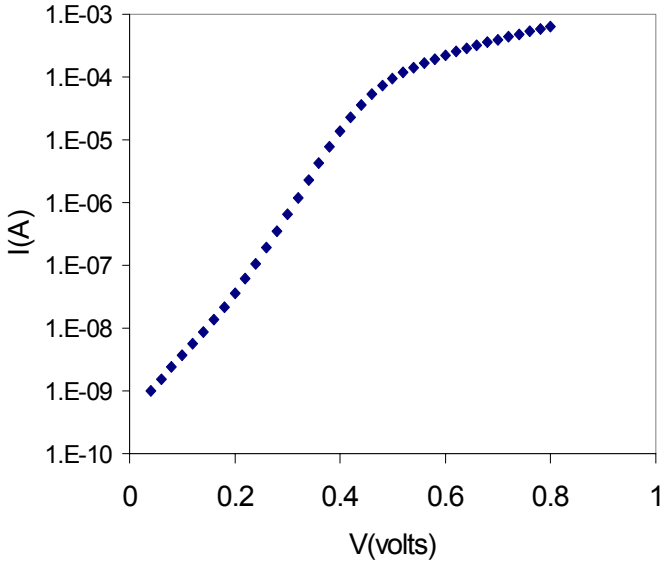
1.E-03
1.E-04
1.E-05
1.E-06
1.E-07
1.E-08
1.E-09
1.E-10
I(A)
0
0.2
0.4
0.6
0.8
1
V(volts)

Fig. 14

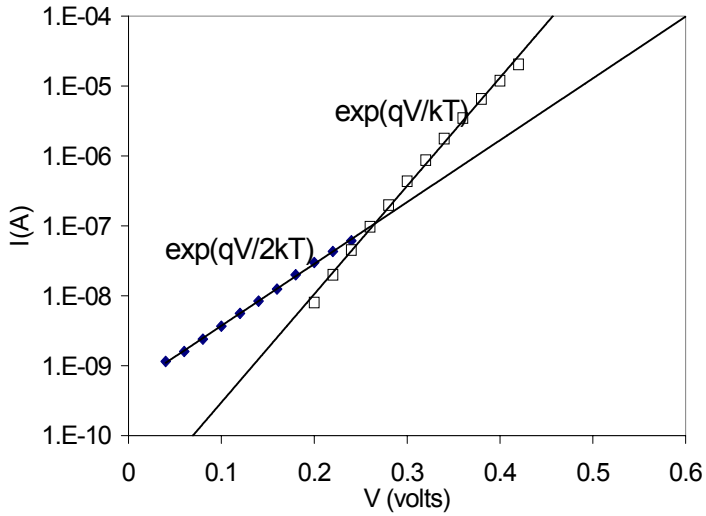
1.E-04
1.E-05
1.E-06
1.E-07
1.E-08
1.E-09
1.E-10
I(A)
exp(qV/kT)
exp(qV/2kT)
0
0.1
0.2
0.3
0.4
0.5
0.6
V (volts)

Appendix 3

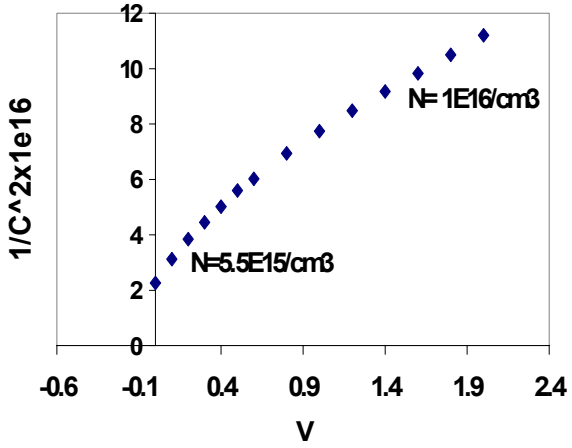

Fig. 1. Graph showing relationship between deep defect densities and shallow defect densities in nanocrystalline Si devices deposited using VHF plasma deposition

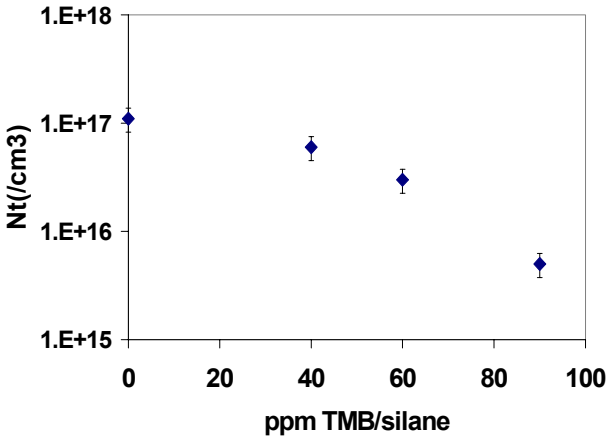

Fig. 2 Relationship between deep defects and compensation by B using TMB as compensating gas feed source in nanocrystalline Si devices.

Appendix 4

Growth and Properties of Amorphous Ge:H Solar cells

Jianhua Zhu*, Vikram L. Dalal*, M. A. Ring,*, James J. Gutierrez+ and J. David Cohen+
*Dept. of Electrical and Computer Engr. and Microelectronics Research Center
Iowa State University, Ames, Iowa 50011, USA
+ Dept. of physics, University of Oregon, Eugene, OR, USA

Abstract

We report on the growth and properties of a-Ge:H materials and solar cells. The materials and cells were grown using remote ECR plasma deposition with high (~50:1) hydrogen dilution. Both p-i-n and n-i-n structures were made with this material on stainless steel substrates. The solar cells showed reasonable fill factors (59%). The measurement of subgap quantum efficiency revealed that the Urbach energy of valence band tails in devices was also very low, being ~43 meV. Measurement of space charge limited current in n-i-n structures showed that the midgap defect density was in the mid-$10^{16}/cm^3$-eV range. Defect densities in the range of mid $10^{16}/cm^3$ were also measured using drive level capacitance, and they were in agreement with SCLC results. Graded bandgap cells were made with this material. They showed an increase in voltage to 0.47 V when appropriate buffer layers were used. These results indicate that good quality a-Ge:H can be made for potential applications in solar cells and image sensors.

Introduction:

Amorphous (Si,Ge):H alloys are now extensively used for photovoltaic devices[1-5]. Generally, the Tauc bandgap of these alloys is restricted to be above 1.45 eV, since the material properties seem to degrade significantly below these bandgap values. We showed in earlier papers that by using appropriate low pressure ECR plasma processes to grow a-(Si,Ge):H alloys, one could make reasonable quality alloys down to a bandgap of ~1.27 eV[6,7]. In this paper, we show that by using very high hydrogen dilution, one can make good materials and devices even in a-Ge:H. A-Ge:H is an interesting material in its own right, both for photovoltaic devices, and for CMOS infrared image sensors.

Growth Techniques

The basic principles of the growth technique used have been described previously [6,7]. Briefly, it consists of using a remote, low pressure ECR plasma process to generate an intense hydrogen plasma. The plasma beam travels downstream towards the substrate, which is remote (25 cm) from the resonance zone of the ECR chamber. Germane gas, diluted either 10% or 20% in hydrogen is introduced near the substrate. Very high dilution ratios are used to produce the films and devices, with typical ratio of hydrogen/germane being >50:1. The pressures in the rector are kept low (5-10 mT) so as to allow for a significant flux of hydrogen ions and radicals to bombard the substrate during growth [6,7]. Typical growth temperatures were in the range of 250-275 °C. Higher temperatures resulted in a deterioration in film and device properties. It is found that using such high dilutions results in the growth being in the "exhaustion regime", where the supply of germane radicals is exhausted. To increase the growth rate, one must increase the germane flow; increasing power does not increase the growth rate.

Results

A. Results on film properties

The films were deposited on Corning 7059 substrates. They were measured for their optical properties using a spectro-photometer, and for their electronic properties using a parallel electrode geometry. Photo and dark conductivity and activation energy were measured. Subgap absorption spectra were measured using a double-beam photo-conductivity technique where a dc beam was used to fix the positions of the quasi Fermi levels and an ac monochromatic beam was used to measure the subgap absorption coefficients. The Tauc bandgap for the films were typically 1.12 eV. The Urbach energy of valence band tails determined from subgap data is remarkably low, ~ 45-46 meV, as described earlier [7]. For comparison, in the best a-Si:H, we obtain a value of ~42-43 meV.

B. Results on space charge limited current in nin structures

nin structures were deposited on stainless steel substrates for defect density measurements. To match the bandgaps and to prevent any notches in band edges at the

interface between the injecting contact and the intrinsic layer, a low gap (~1.4 eV) a-(Si,Ge):H n layer was used as the injecting contacts. If, instead of such a low gap a-(Si,Ge):H n layer, an a-Si:H n layer was used, it led to non-injecting contacts, as demonstrated by non-equality of the I(V) curves under different polarities. For the polarity where the a-Si:H n layer was the injecting contact, the current was always lower than when the a-(Si,Ge):H n layer was the injecting contact. In contrast, when both n layers were made from a-(Si,Ge):H, the curves were essentially symmetrical in polarity. See Fig. 1 for a typical I(V) curve under both polarities.

From such I(V) curves, one can estimate the midgap defect density as being $3x10^{16}/cm^3$-eV, using the point-by-point method of den Boer [8].

C. Results on drive-level capacitance on Schottky/i/n devices.

A series of samples were made identical to the SCLC samples, and were measured at University of Oregon using derive-level capacitance techniques [9]. In Fig. 2, we show the results of such measurements which indicate a low defect density, in the mid $10^{16}/cm^3$, in agreement with SCLC results.

D. Results on pin devices

pin devices were deposited on stainless steel substrates, using the ECR process. P layers were doped using diborane, and n layers using phosphine. The devices generally had an a-Si:H n layer, followed by a thin (~20 nm) graded gap region to match the band edges of the n layer with the band edges of i-a-Ge:H. The thickness of the a-Ge:H layer was typically ~150-200 nm. The i a-Ge:H layer was followed by a graded gap buffer layer to match with the band edges of the p a-(Si,C):H layer, and to reduce interfacial recombination. The buffer layer was followed by an a-(Si,C):H p layer.No back reflector was used. ITO contacts were provided on top of the p layer.

In Fig. 3, we show the illuminated I(V) curve, measured under AM1.5 condition, for a typical solar cell. The fill factor is quite good (59%), a value expected given the level of defect density in the material. Obviously, the material is not as good as a-Si:H, where the defect density is in the mid $10^{15}/cm^3$ range. The open-circuit voltage is 0.40 V, a value which agrees with the low bandgap of the material. The current density is 14 mA/cm^2. The corresponding quantum efficiency (QE) curve is shown in Fig.4, where we show that the QE extends out to 900 nm, clearly showing the value of a low bandgap. An extended curve for subgap QE vs. photon energy is shown in Fig. 5. The value for Urbach energy for valence band tails can be determined from this curve [9], and it is ~43 meV, a very low value, implying a high quality material.

We also fabricated graded bandgap cells in this material. The bandgap was graded from a-Si:H to a-Ge:H in a smooth fashion over the first ~100nm of the i layer. The last 100 nm was only a-Ge:H. The graded gap cell showed an improved voltage(0.43V) compared to the a-Ge:H device by itself. The voltage can be further improved by

increasing the thickness of the graded gap buffer layer between the i and p layers. When this was done, the voltage improved to 0.47 V (See Fig. 6). Of course, the improvement in voltage upon grading the bandgap of the i layer comes at the expense of QE at 800-900 nm, as shown in Fig. 7. The fill factor of 55% is slightly worse. A subgap absorption curve for this cell shows that the implied Urbach energy is again very low, 42 meV. Of course, in a graded i layer gap structure like this, one cannot accurately determine the Urbach energy, since different bandgap layers may have different values of Urbach energy.

Finally, we estimated the hole mobility-lifetime ($\mu\tau$) product in an a-Ge:H cell from quantum efficiency vs. voltage measurements (See Fig.8). From such curves, one can estimate the hole ($\mu\tau$) product to be ~$4x10^{-9}$ cm^2/V, which is smaller than the value in a-Si:H, which is typically ~$2\text{-}3x10^{-8}$ cm^2/V. The lower value in a-Ge:H agrees with the much higher defect density in the material (~$3 \times 10^{16}/cm^3$) compared to a-Si:H.

Discussion

From the above results, we have shown that when a-Ge:H is made using an " exhaustion" regime, with high hydrogen dilution, one obtains a reasonable quality material. The quality of the material, while good, is still inferior to that of a-Si:H. For example, the defect densities are higher by about a factor of 6, and the Urbach energies are also slightly higher. These higher defects result in a lower fill factor for devices (59%) and in a lower hole ($\mu\tau$) product by about a factor of 6 when compared with a-Si:H. Clearly, more work needs to be done to demonstrate the potential of a-Ge:H for both image sensing and photovoltaic applications.

Conclusions

In conclusion, we have shown that reasonable quality a-Ge:H materials and p-i-n cells can be made by carefully controlling the plasma properties. An exhaustion regime of plasma, where there is an excess of hydrogen present, is needed to produce the best films and devices. Low pressures are necessary in order to have significant ion bombardment present. The Urbach energies are quite low, in the range of 43-45 meV in both materials and devices. The defect densities measured using both subgap absorption and space charge limited current are in the mid $10^{16}/cm^3$ range. Fill factors in devices are reasonable (59%). The hole ($\mu\tau$) products are ~$4x10^{-9}$ cm^2/V, about a factor of 6 lower than in a-Si:H.

Acknowledgements

It is a pleasure to thank Kay Han and Puneet Sharma for their technical help. This work was partially supported by NREL.

Figure Captions

1. Space charge limited current data for nin a-Ge:H sample. The mid-level defect density estimated from this measurement is 2-3 x $10^{16}/cm^3$-eV over the range of voltages studied.

2. Defect density determined from drive level capacitance studies in Schottky barrier structures deposited on materials similar to those used in Fig. 1.

3. Device I(V) curve for a pin a-Ge:H solar cell. The votlage is 0.4 V, the fill factor is 59% and the current density is 14 mA/cm^2. No back reflector is used.

4. QE data for the cell of Fig. 3

5. Subgap QE data for the cell of Fig. 3. The Urbach energy of valence band tails, estimated from the QE data, is 43 meV.

6. I(V) curve of a cell with graded bandgap and with a p-i buffer layer which is thicker than for the cell of Fig. 3. The open-circuit voltage has increased to 0.47 V.

7. QE data for the cell of Fig.6, showing a slight decrease in QE compared to the ungraded cell whose QE data was shown in Fig. 4.

8. QE vs. voltage data for a-Ge:H cell showing a fit with a mobility-lifetime product of $4x10^{-9}$ cm^2/V.

References:

1. Subhendu Guha, Jeffrey Yang, Arindam Banerjee, Baojie Yan and Kenneth Lord, Solar Energy Mater. And Solar cells, 78, 329-347,(2003)

2. D. E. Carlson, Solar Energy Mater. And Solar cells, 78, 627(2003)

3. Masat Izu and Tim Ellison, Solar Energy Mater. And Solar cells, 78,613(2003)

4. R. J. Zambrano, F. A. Rubinelli, J. K. Ratha nd R. E. I. Schropp, J. Non-cryst. Solids, 299-302, 1131(2001)

5. Jeffrey Yang, Arindam Banerjee and Subhendu Guha, Solar Energy Mater. And Solar cells, 78,597(2003)

6. Vikram L. Dalal, Yong Liu , Zhiyang Zhou and Keqin Han, , J. Non-Cryst. Solids, 299-302, 1127(2002)

7. Vikram Dalal and Yong Liu, " Properties of low gap a-Si,Ge materials and devices", Proc. Of 29th. IEEE Photovolt. Conf.(2002)

8. W. den Boer, J. de Physique(Paris) 42,C-4, 485(1981)

9. J. D. Cohen, Solar Energy Mater. And Solar cells, 78, 399(2003)

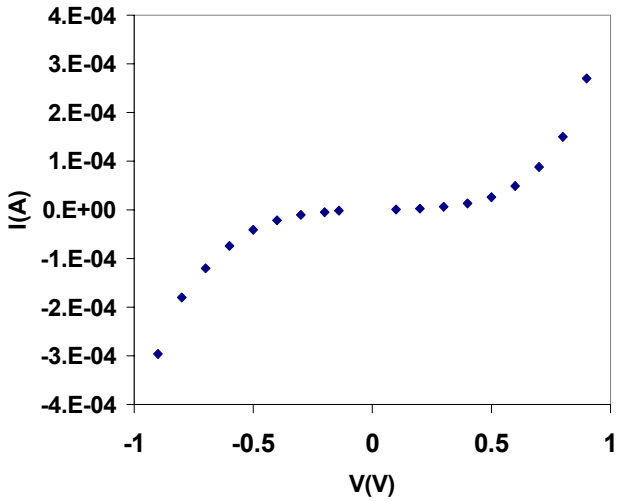

Fig. 1

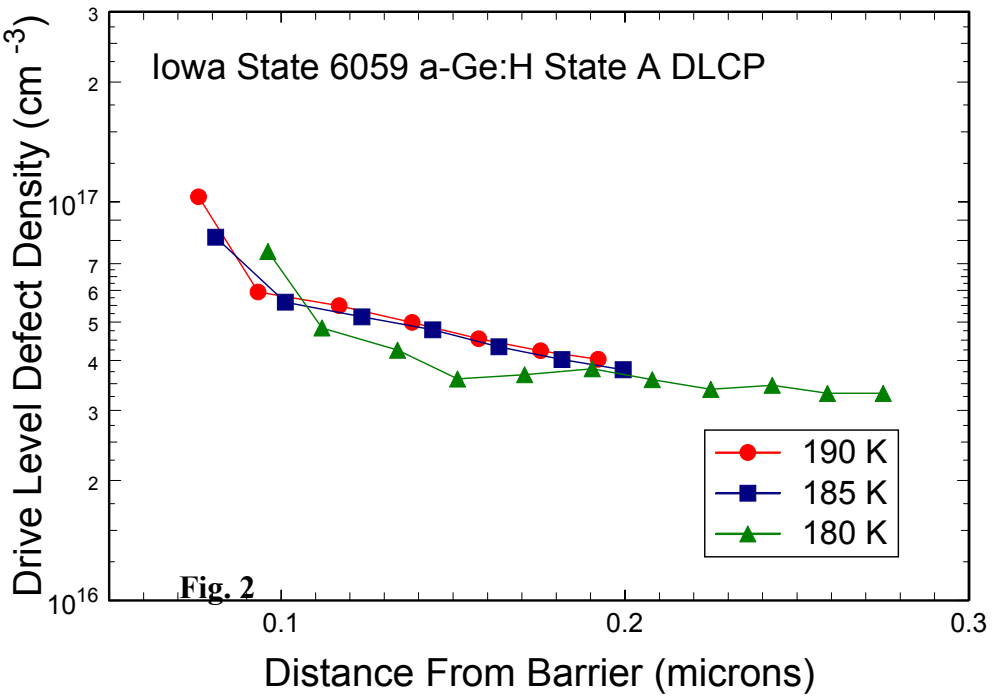
Iowa State 6059 a-Ge:H State A DLCP
Drive Level Defect Density (cm -3)
Distance From Barrier (microns)
190 K
185 K
180 K
3
2
10^17
7
6
5
4
3
2
10^16
0.1
0.2
0.3

Fig. 2

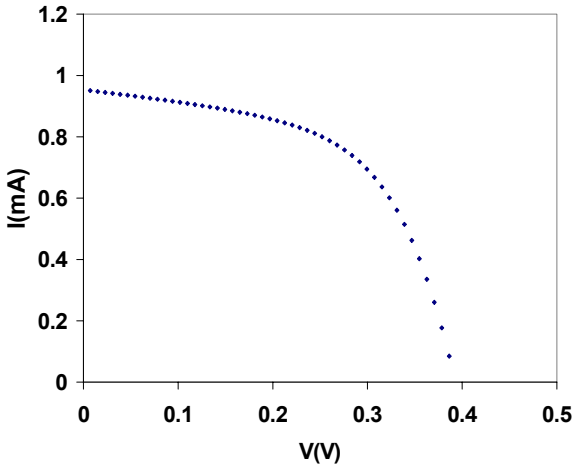

Fig. 3

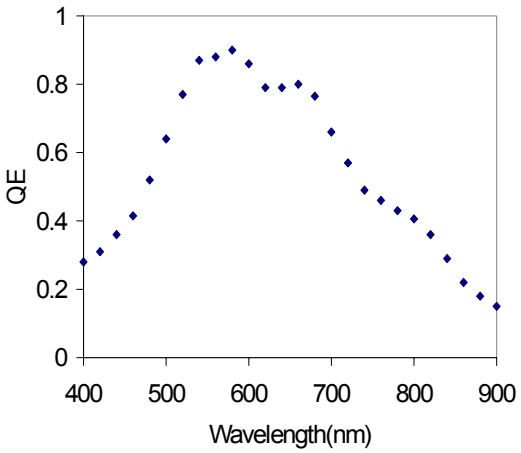

Fig. 4

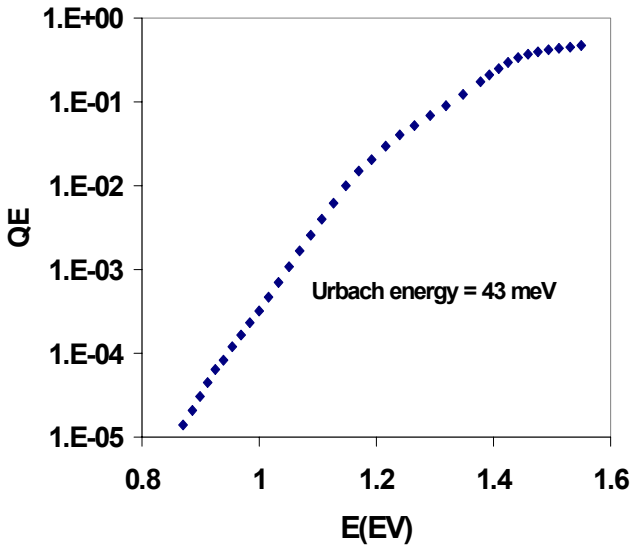
1.E+00
1.E-01
1.E-02
1.E-03
1.E-04
1.E-05
QE
Urbach energy = 43 meV
0.8
1
1.2
1.4
1.6
E(EV)

Fig. 5

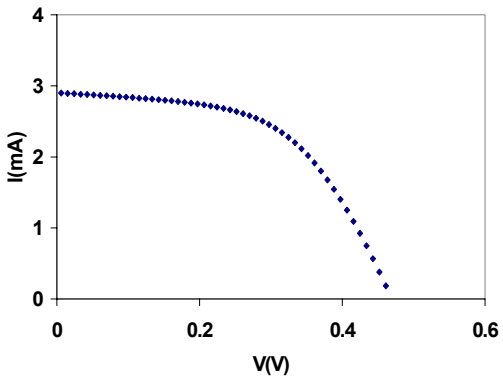

Fig. 6

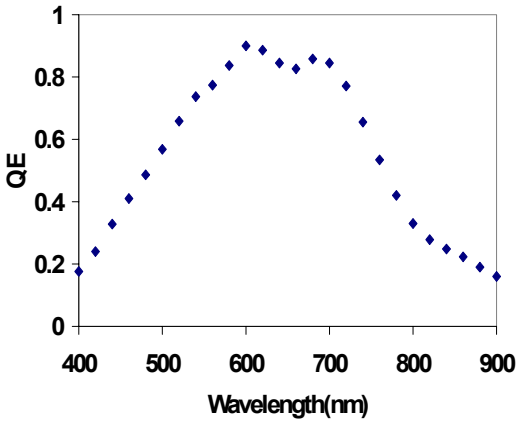

Fig. 7

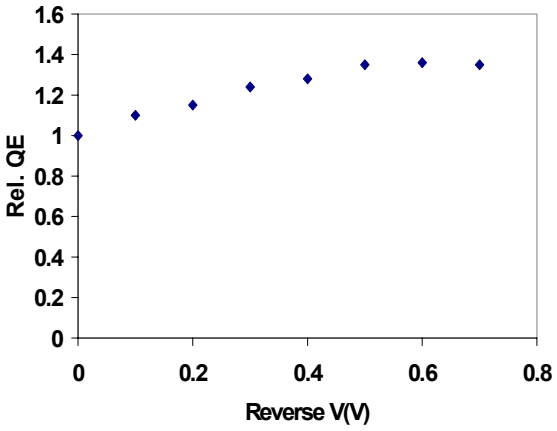

Fig. 8

Appendix 5

Diffusion length of holes in MV systems nanocrystalline Si devices